Heavy Quarkonium in a Holographic Basis

Yang Li[a,*], Pieter Maris[a], Xingbo Zhao[b], James P. Vary[a]

[a] *Department of Physics and Astronomy, Iowa State University, Ames, IA 50011, USA*

[b] *Institute of Modern Physics, Chinese Academy of Sciences, Lanzhou 730000, China*

arXiv:1509.07212v3 [hep-ph] 10 May 2016

Abstract

We study the heavy quarkonium within the basis light-front quantization approach. We implement the one-gluon exchange interaction and a confining potential inspired by light-front holography. We adopt the holographic light-front wavefunction (LFWF) as our basis function and solve the non-perturbative dynamics by diagonalizing the Hamiltonian matrix. We obtain the mass spectrum for charmonium and bottomonium. With the obtained LFWFs, we also compute the decay constants and the charge form factors for selected eigenstates. The results are compared with the experimental measurements and with other established methods.

Keywords: heavy quarkonium, light front, holographic QCD, spectroscopy, decay constant, form factor

1. Introduction

Describing hadrons from quantum chromodynamics (QCD) remains a fundamental challenge in nuclear physics. Inspired by the discovery of a remarkable gauge/string duality [1], holographic QCD models, most notably the AdS/QCD [2], have been proposed as analytic semi-classical approximations to QCD (for a recent review, see Ref. [3]). In light of these phenomenological successes, as well as the recent progress in the *ab initio* nuclear structure calculations [4–7], the basis light-front quantization (BLFQ) [8] has been developed as a non-perturbative approach to address QCD bound-state problems from first principles.

BLFQ is based on the Hamiltonian formalism in light-front dynamics (LFD, [9]) in Minkowski space. The central task of the Hamiltonian approach is to diagonalize the QCD Hamiltonian operator,

$$P^+\hat{P}^-|\psi_h\rangle = M_h^2|\psi_h\rangle. \tag{1}$$

Here $P^\pm = P^0 \pm P^3$ is the longitudinal momentum and the light-front quantized Hamiltonian operator, respectively. The eigenvalues directly produce the invariant-mass spectrum. The eigenfunctions, known as the light-front wavefunctions (LFWFs), play a pivotal role in the study of the hadron structures in deep inelastic scattering (DIS) [10] and deeply virtually Compton scattering (DVCS) [11]. In the Fock space expansion, Eq. (1) becomes a relativistic quantum many-body problem and can be solved by constructing and diagonalizing the many-body Hamiltonian matrix (see, e.g., [12] for a review).

The advantages of LFD are made explicit by BLFQ which can employ an arbitrary single-particle basis subject to completeness and orthonormality. By adopting a single-particle AdS/QCD basis, BLFQ naturally extends the AdS/QCD LFWFs to the multi-particle Fock sectors [8]. Furthermore, this basis preserves all the kinematical symmetries of the full Hamiltonian [13, 14]. Such choice is in parallel with the no-core shell model (NCSM) used in non-relativistic quantum many-body theory [5]. State-of-the-art computational tools developed in the many-body theory can be used to address the QCD eigenvalue problem [15]. BLFQ has been applied successfully to a range of non-perturbative problems,

*Corresponding author

Email addresses: leeyoung@iastate.edu (Yang Li), pmaris@iastate.edu (Pieter Maris), xbzhao@impcas.ac.cn (Xingbo Zhao), jvary@iastate.edu (James P. Vary)

including the electron anomalous magnetic moment [16, 17], non-linear Compton scattering [18, 19] and the positronium spectrum [20, 21]. In this paper, we apply the BLFQ approach to the heavy quarkonium.

Working with the full QCD Hamiltonian is a formidable task. In practice, we truncate the Fock space to a finite number of particles. The leading-order truncation $|q\bar{q}\rangle + |q\bar{q}g\rangle$ introduces the one-gluon exchange which produces correct short-distance physics as well as the spin-dependent interaction needed for the fine and hyperfine structures. The Abelian version of this interaction was extensively used in the literature [20, 22–25] to calculate the QED bound-state spectrum in LFD. However, the one-gluon exchange itself is not sufficient to reproduce the hadron spectrum since confinement is also needed. Holographic QCD provides an appealing approximation to confinement.

Heavy quarkonium is an ideal laboratory for studying non-perturbative aspects of QCD and their interplay with the perturbative physics [26]. Conventional theoretical tools include the non-relativistic potential models (NRPMs) [27, 28], non-relativistic QCD (NRQCD) [29], heavy quark effective field theory [30], Dyson-Schwinger Equations (DSE) [31–34], and Lattice QCD [35]. The recent discoveries of tetraquark [36] and pentaquark [37] states have renewed interests in the theoretical investigation of heavy quarkonium. Extensive data on heavy quarkonium have been produced by experimental facilities, such as Belle, CLEO and LHC.

Numerous light-front phenomenologies have been developed for heavy quarkonium (see e.g. [38–44] and the references therein). Our approach shares some similarity with these models. Yet, there are also major differences. First of all, our approach employs holographic QCD (confining interaction) and realistic LFQCD (one-gluon exchange). Secondly and most importantly, we solve quarkonium as a two-body bound-state problem using a Hamiltonian method that is applicable to arbitrary many-body bound states, once the (effective) Hamiltonian and the basis space are specified. We exploit the fact that BLFQ is developed as a flexible computational platform for relativistic strong interaction many-body bound-state problems [8, 15], designed to deal with general Hamiltonians, realistic or phenomenological.

Our goal in this work can be simply stated: we aim to improve the light-front holographic QCD results [45] by including a realistic one-gluon exchange interaction. Computationally, we intend to lay the foundation for the extension to higher Fock sectors.

2. Effective Hamiltonian

2.1. Phenomenological confinement

Our effective Hamiltonian consists of the holographic QCD Hamiltonian and the one-gluon exchange. We adopt the light-front AdS/QCD soft-wall (SW) Hamiltonian for the first part [46]. This simple model gives a reasonable description of the hadron spectrum and structures (see Ref. [45] for a review). Its effective "light-cone" Hamiltonian reads,

$$H_{\rm sw} \equiv P^+ \hat{P}^-_{\rm sw} - \boldsymbol{P}_\perp^2 = \frac{\boldsymbol{k}_\perp^2}{x(1-x)} + \kappa^4 x(1-x)\boldsymbol{r}_\perp^2, \tag{2}$$

where, $x = p_q^+/P^+$ is the longitudinal momentum fraction of the quark, $\boldsymbol{k}_\perp = \boldsymbol{p}_{q\perp} - x\boldsymbol{P}_\perp$ is the relative transverse momentum, and $\boldsymbol{r}_\perp$ is the transverse separation of the partons. κ is the strength of the confining potential. Note that the "light-cone Hamiltonian" has mass squared dimension, whose eigenvalues are the squared invariant masses. Following Brodsky and de Téramond [46], it is convenient to introduce the holographic coordinate $\boldsymbol{\zeta}_\perp = \sqrt{x(1-x)}\boldsymbol{r}_\perp$, and its conjugate $\boldsymbol{q}_\perp = \boldsymbol{k}_\perp/\sqrt{x(1-x)} \equiv -i\nabla_{\zeta_\perp}$. In light-front holography, $\zeta_\perp$ is mapped to the fifth coordinate z of the AdS space. In these coordinates, $H_{\rm sw}$ is a harmonic oscillator (HO),

$$H_{\rm sw} = \boldsymbol{q}_\perp^2 + \kappa^4 \boldsymbol{\zeta}_\perp^2. \tag{3}$$

Its eigenvalues follow the Regge trajectory $M^2 = 2\kappa^2(2n + |m| + 1)$. Its eigenfunctions are 2D HO functions in the holographic variables,

$$\phi_{nm}(\boldsymbol{q}_\perp) = e^{im\theta}\left(\frac{q_\perp}{\kappa}\right)^{|m|} e^{-q_\perp^2/(2\kappa^2)} L_n^{|m|}(q_\perp^2/\kappa^2). \tag{4}$$

Here $q_\perp = |\boldsymbol{q}_\perp|$, $\theta = \arg \boldsymbol{q}_\perp$, and $L_n^m(z)$ is the associated Laguerre polynomial. We adopt these functions as our basis. This basis has the advantage that in the many-body sector, it allows the exact factorization of the center-of-mass motion in the single-particle coordinates. This is a very valuable property, because the boson/fermion symmetrization/anti-symmetrization in the relative coordinates quickly becomes intractable, as the number of identical particles increases [13, 14]. For this work, however, we do not have identical particles in the $q\bar{q}$ sector and we will use the relative coordinate. In future extensions, as sea quarks and gluons are added, it may be more advantageous to adopt single-particle coordinates.

The soft-wall Hamiltonian Eq. (3) is designed for massless quarks, and it is inherently 2-dimensional. For the heavy quarkonium systems, it should be modified to incorporate the quark masses and the longitudinal dynamics,

$$H_{\rm SW} \to H_{\rm CON} = \boldsymbol{q}_\perp^2 + \kappa^4 \boldsymbol{\zeta}_\perp^2 + \frac{m_q^2}{x} + \frac{m_{\bar{q}}^2}{1-x} + V_L(x). \tag{5}$$

Here V_L is a longitudinal confining potential. Several longitudinal confining potentials have been proposed [47–49]. Here we propose a new longitudinal confinement which shares features with others proposed,

$$V_L(x) = -\frac{\kappa^4}{(m_q + m_{\bar{q}})^2} \partial_x \big(x(1-x)\partial_x \big), \tag{6}$$

where $\partial_x \equiv (\partial/\partial x)_{\boldsymbol{\zeta}_\perp}$. This term combined with the mass term from the kinetic energy forms a Sturm-Liouville problem,

$$-\partial_x \big(x(1-x)\partial_x \chi_l(x) \big) + \frac{1}{4}\Big(\frac{\alpha^2}{1-x} + \frac{\beta^2}{x} \Big) \chi_l(x) = \lambda_l^{(\alpha,\beta)} \chi_l(x), \tag{7}$$

where $\alpha = 2m_{\bar{q}}(m_q + m_{\bar{q}})/\kappa^2$, $\beta = 2m_q(m_q + m_{\bar{q}})/\kappa^2$. The solutions of Eq. (7) are analytically known in terms of the Jacobi polynomial $P_l^{(a,b)}(z)$,

$$\chi_l(x) = x^{\frac{1}{2}\alpha}(1-x)^{\frac{1}{2}\beta} P_l^{(\alpha,\beta)}(2x-1). \tag{8}$$

and form a complete orthogonal basis on the interval $[0,1]$. The corresponding eigenvalues are

$$\lambda_l^{(\alpha,\beta)} = (l + \tfrac{1}{2}(\alpha+\beta))(l + \tfrac{1}{2}(\alpha+\beta) + 1). \quad (l = 0, 1, 2, \cdots) \tag{9}$$

Comparing to other forms of longitudinal confinement, our proposal implements several attractive features. First, the basis functions resemble the known asymptotic parton distribution $\sim x^\alpha(1-x)^\beta$ with $\alpha, \beta > 0$ [50]. This is our primary motivation for adopting the longitudinal confinement Eq. (6). Second, the basis function is also analytically known, which brings numerical convenience. Third, in the non-relativistic limit $\min\{m_q, m_{\bar{q}}\} \gg \kappa$, the longitudinal confinement sits on equal footing with the transverse confinement, where together, they form a 3D harmonic oscillator potential,

$$V_{\rm con} = \frac{m_q m_{\bar{q}}}{(m_q + m_{\bar{q}})^2} \kappa^4 \boldsymbol{r}^2, \tag{10}$$

and rotational symmetry is manifest. This non-relativistic reduction also provides us an order-of-magnitude estimate of the model parameters for our heavy quarkonium application. Fourth, in the massless limit $\max\{m_q, m_{\bar{q}}\} \ll \kappa$, the longitudinal mode stays in the ground state and the longitudinal wavefunction $\chi_0(x) = \text{const}$. Thus we restore the massless model of Brodsky and de Téramond[1].

2.2. One-Gluon exchange

Following Ref. [20] (cf. [22–25]), we introduce the one-gluon exchange in LFD. In the momentum space, this term reads,

$$\langle \boldsymbol{k}'_\perp, x', s', \bar{s}' | V_{\rm g} | \boldsymbol{k}_\perp, x, s, \bar{s} \rangle = -\frac{4}{3} \times \frac{4\pi\alpha_s}{Q^2} S_{s,\bar{s},s',\bar{s}'}(\boldsymbol{k}_\perp, x, \boldsymbol{k}'_\perp, x') \tag{11}$$

[1] Note that in our normalization convention, the LFWFs differ from Brodsky et al.'s [45] by a factor $\sqrt{x(1-x)}$.

where $S_{s,\bar{s},s',\bar{s}'}(\boldsymbol{k}_\perp, x, \boldsymbol{k}'_\perp, x') = \bar{u}_{s'}(\boldsymbol{k}'_\perp, x')\gamma_\mu u_s(\boldsymbol{k}_\perp, x)\bar{v}_{\bar{s}}(-\boldsymbol{k}_\perp, 1-x)\gamma^\mu v_{\bar{s}'}(-\boldsymbol{k}'_\perp, 1-x')$, and, $Q^2 = \frac{1}{2}\left(\sqrt{\frac{x'}{x}}\boldsymbol{k}_\perp - \sqrt{\frac{x}{x'}}\boldsymbol{k}'_\perp\right)^2 + \frac{1}{2}\left(\sqrt{\frac{1-x'}{1-x}}\boldsymbol{k}_\perp - \sqrt{\frac{1-x}{1-x'}}\boldsymbol{k}'_\perp\right)^2 + \frac{1}{2}(x-x')^2\left(\frac{m_q^2}{xx'} + \frac{m_{\bar{q}}^2}{(1-x)(1-x')}\right) + \mu_g^2$, is the average momentum transfer. We have also introduced a gluon mass μ_g to regularize the Coulomb singularity. This singularity is integrable and does not carry physical significance. The gluon mass is used to improve the numerics and will be taken small compared to other scales in this application. In Eq. (11), we have taken the total momentum $\boldsymbol{P}_\perp = 0, P^+ = 1$ by virtue of the boost invariance in LFD.

This one-gluon exchange introduces a logarithmic divergence [21, 23, 25, 51]. This can be seen from the one-gluon exchange kernel by transverse power counting. In particular, the leading power comes from the spin non-flip spinor matrix elements $S_{\uparrow\downarrow\uparrow\downarrow}$ and $S_{\downarrow\uparrow\downarrow\uparrow}$, which contain terms proportional to $\boldsymbol{k}_\perp^2$ or $\boldsymbol{k}_\perp'^2$. Such terms do not vanish in the large momentum limit[2]. In principle, this divergence can be handled by a proper renormalization [52–56]. However, such a procedure is usually rather challenging or even impractical. In this work, we adopt a simple counterterm technique [20, 21, 23, 24, 51] by replacing the spinor matrix elements $S_{\uparrow\downarrow\uparrow\downarrow}$ and $S_{\downarrow\uparrow\downarrow\uparrow}$ with,

$$S_{s,\bar{s},s',\bar{s}'}(\boldsymbol{k}_\perp, x, \boldsymbol{k}'_\perp, x') \to S_{s,\bar{s},s',\bar{s}'}(\boldsymbol{k}_\perp, x, \boldsymbol{k}'_\perp, x') - 2\boldsymbol{k}_\perp^2\sqrt{\frac{x'(1-x')}{x(1-x)}} - 2\boldsymbol{k}_\perp'^2\sqrt{\frac{x(1-x)}{x'(1-x')}}. \quad (s,\bar{s},s',\bar{s}' = \uparrow\downarrow\uparrow\downarrow \text{ or } \downarrow\uparrow\downarrow\uparrow) \quad (12)$$

In its essence, this counterterm exactly removes the troubling $\boldsymbol{k}_\perp^2$ and $\boldsymbol{k}_\perp'^2$ terms in the spinor matrix elements hence removing the UV divergence.

3. Basis light-front quantization

In Sect. 2, we derived the effective light-cone Hamiltonian operator for quarkonium, which reads,

$$H_{\text{eff}} = \boldsymbol{q}_\perp^2 + \kappa^4\boldsymbol{\zeta}_\perp^2 + \frac{m_q^2}{x} + \frac{m_{\bar{q}}^2}{1-x} - \frac{\kappa^4}{(m_q+m_{\bar{q}})^2}\partial_x\big(x(1-x)\partial_x\big) + V_{\text{g}}. \quad (13)$$

In this section, we will focus on solving the eigenvalue equation non-perturbatively,

$$H_{\text{eff}}\,|\psi_{m_J}^{J^{PC}}\rangle = M^2|\psi_{m_J}^{J^{PC}}\rangle, \quad (14)$$

to obtain the mass spectrum and the LFWFs $\psi_{m_J}^J(\boldsymbol{k}_\perp, x, s, \bar{s}) \equiv \langle \boldsymbol{k}_\perp, x, s, \bar{s}|\psi_{m_J}^{J^{PC}}\rangle$. Here J, P, C and m_J are the total spin, parity, charge parity, and the magnetic projection of the state, respectively. Our strategy is to construct a finite-dimensional matrix from the effective Hamiltonian operator and then diagonalize it numerically. To do this, we first adopt a basis expansion,

$$\psi_{m_J}^J(\boldsymbol{k}_\perp, x, s, \bar{s}) = \sum_{n,m,l}\delta_{m_J,m+s+\bar{s}}\,\widetilde{\psi}_{m_J}^J(n,m,l,s,\bar{s})\,\Phi_{nml}(\boldsymbol{k}_\perp/\sqrt{x(1-x)}, x). \quad (15)$$

Here $\widetilde{\psi}_{m_J}^J(n,m,l,s,\bar{s}) \equiv \langle n,m,l,s,\bar{s}|\psi_{m_J}^{J^{PC}}\rangle$ are the LFWFs in the BLFQ basis. As mentioned above, the basis functions $\Phi_{nml}(\boldsymbol{q}_\perp, x) \equiv \phi_{nm}(\boldsymbol{q}_\perp)\chi_l(x)$ are generated by the confining part of the Hamiltonian – the kinematic energy plus the confinement. As such, the light-front holographic QCD results serve as our first approximation. The matrix elements of the Hamiltonian within this basis are,

$$\begin{aligned}\langle n',m',l',s',\bar{s}'|H_{\text{eff}}|n,m,l,s,\bar{s}\rangle &= \langle n',m',l',s',\bar{s}'|V_{\text{g}}|n,m,l,s,\bar{s}\rangle \\ &+ \Big[(m_q+m_{\bar{q}})^2 + 2\kappa^2(2n+|m|+l+\tfrac{3}{2}) + \frac{\kappa^4}{(m_q+m_{\bar{q}})^2}l(l+1)\Big]\delta_{nn'}\delta_{mm'}\delta_{ll'}\delta_{ss'}\delta_{\bar{s}\bar{s}'}. \quad (16)\end{aligned}$$

We take advantage of the conservation of the angular momentum in the transverse plane, and choose a particular magnetic projection m_J: $m + s + \bar{s} = m_J$. In order to carry out practical calculations,

[2] From the perturbative point of view, this should be canceled by a similar contribution in the cross ladder diagram, which is absent from our Fock space.

we truncate the infinite basis space to a finite size by restricting the quantum numbers according to $2n+|m|+1 \leq N_{\max}, l \leq L_{\max}$. $N_{\max}$ controls the range of momenta covered by the harmonic oscillator basis as it is related to a transverse IR regulator $\lambda_{\rm IR} \sim b/\sqrt{N_{\max}}$ and a UV regulator $\Lambda_{\rm UV} \sim \sqrt{N_{\max}}b$ [57], where b is the HO basis scale and we have taken $b = \kappa$, unless otherwise stated. $L_{\max}$ controls the basis resolution in the longitudinal direction.

The relativistic bound states are identified by three quantum numbers J^{PC}. However, P is broken by the finite basis truncation, because the parity transformation is dynamical in LFD. Instead, one can exploit the so-called mirror parity $\hat{P}_x = \hat{R}_x(\pi)\hat{P}$ that is related to P [58],

$$\hat{P}_x|\psi^{J^{PC}}_{m_J}\rangle = (-1)^J P|\psi^{J^{PC}}_{-m_J}\rangle. \tag{17}$$

Then P can be extracted from the LFWFs by,

$$(-1)^J P = \langle\psi^{J^{PC}}_{-m_J}|\hat{R}_x(\pi)\hat{P}|\psi^{J^{PC}}_{m_J}\rangle = \sum_{n,m,l,s,\bar{s}} (-1)^m\, \widetilde{\psi}^{J*}_{-m_J}(n,-m,l,-s,-\bar{s})\widetilde{\psi}^{J}_{m_J}(n,m,l,s,\bar{s}). \tag{18}$$

Similarly, C can be obtained from the LFWFs by,

$$C = \langle\psi^{J^{PC}}_{m_J}|\hat{C}|\psi^{J^{PC}}_{m_J}\rangle = \sum_{n,m,l,s,\bar{s}} (-1)^{m+l+1}\, \widetilde{\psi}^{J*}_{m_J}(n,m,l,s,\bar{s})\widetilde{\psi}^{J}_{m_J}(n,m,l,\bar{s},s). \tag{19}$$

Rotation is also a dynamical symmetry in LFD. As a result, J is not conserved and the mass degeneracy for different magnetic projections m_J is lifted by the Fock-space truncation. Nevertheless, in a non-relativistic system, such as the heavy quarkonium, the discrepancy is small and we can still extract J by counting the multiplicity of the nearly-degenerate mass eigenstates. It is also instructive to assign states the non-relativistic quantum numbers $n\,^{2S+1}L_J$, where n, S and L are the radial quantum number, the spin and the orbital angular momentum, respectively. L, S are related to parity and charge conjugation through $P = (-1)^{L+1}, C = (-1)^{L+S}$. The radial quantum number n can be deduced from the mass hierarchy of the spectrum. The total spin S, though not an exact quantum number, can be obtained from its expectation value, $\langle\psi^{J^{PC}}_{m_J}|\vec{S}^2|\psi^{J^{PC}}_{m_J}\rangle = S(S+1)$. L, S, J are constrained by the angular momentum addition $|L-S| \leq J \leq L+S$. Reconstructing these quantum numbers allows us to identify the states and to compare with experimental data and with other methods.

4. Numerical Results

In this work, we focus on charmonium and bottomonium, where the fermion masses are equal ($m_q = m_{\bar{q}}$) and heavy ($m_q \gtrsim \kappa$). The Hamiltonian matrix element (Eq. (16)) involves a four-dimensional integral (two in the radial direction, two in the longitudinal direction). They are evaluated using Gauss quadratures. The number of the quadrature points $N_{\rm rad}$ ($N_{\rm lfx}$) is taken to be at least twice $N_{\max}$ ($L_{\max}$). Then the obtained matrix is diagonalized using LAPACK software [59]. We fix the bottomonium coupling $\alpha_s(M_{b\bar{b}}) = 0.25$ and obtain the charmonium coupling $\alpha_s(M_{c\bar{c}}) = 0.3595$ using the leading-order pQCD evolution of strong coupling ($N_f = 5, M_{c\bar{c}} \simeq 3.5\,\text{GeV}, M_{b\bar{b}} \simeq 9.5\,\text{GeV}$). We then fit the parameters κ, m_q (m_c, m_b) by minimizing the root-mean-squared (r.m.s.) deviation from the experimental masses [60] of the states below the $D\overline{D}$ or $B\overline{B}$ threshold. The details of the model parameters are summarized in Table 1. In these calculations, we take the regulators $\mu_g = 0.02\,\text{GeV} \ll \kappa$, $N_{\max} = L_{\max} = 8, 16, 24$ ($N_{\max} = 8$ is available in the supplemental materials), and the number of quadrature points $N_{\rm rad} = N_{\rm lfx} = 64$.

Previous BLFQ study of positronium [20, 21] shows that the continuum limit $N_{\max} \to \infty$, $L_{\max} \to \infty$, $\mu_g \to 0$ can be reached through extensive calculation and successive extrapolations. However, we shall not investigate the $N_{\max}$, $L_{\max}$ and μ_g extrapolations in this paper because of the numerical efforts involved and also the presence of several fitted parameters. Comparing the results with $N_{\max} = L_{\max} = 16$ and $N_{\max} = L_{\max} = 24$ in Table 1, where the model parameters κ, m_q were fitted separately and turned out to be very close ($\lesssim 1\%$ change). The r.m.s. deviations from the measured spectra are also comparable. We also studied the trend of the mass eigenvalues with decreasing μ_g in the range of $10^{-4}\,\text{GeV} \leq \mu_g \leq 3\times10^{-1}\,\text{GeV}$ at fixed $N_{\max} = L_{\max}$, and found that the mass eigenvalues are well converged with respect to μ_g.

Table 1: Summary of the model parameters. The coupling α_s and the gluon mass μ_g are fixed (see the text). The confining strength κ and the quark mass m_q are fitted with $m_J = 0$ using the experimental data below the $D\overline{D}$ or $B\overline{B}$ threshold. The r.m.s. deviations for the $m_J = 0$ spectrum, $\delta M_{m_J=0}$, and the r.m.s. average-m_J spectrum, $\delta\overline{M}$, are computed for states below the threshold.

	α_s	μ_g (GeV)	κ (GeV)	m_q (GeV)	$\delta M_{m_J=0}$ (MeV)	$\delta\overline{M}$ (MeV)	$N_{\max} = L_{\max}$
$c\bar{c}$	0.3595	0.02	0.950	1.510	64 (8 states)	52 (8 states)	16
$b\bar{b}$	0.25		1.491	4.761	56 (14 states)	51 (14 states)	
$c\bar{c}$	0.3595	0.02	0.938	1.522	65 (8 states)	52 (8 states)	24
$b\bar{b}$	0.25		1.490	4.763	54 (14 states)	50 (14 states)	

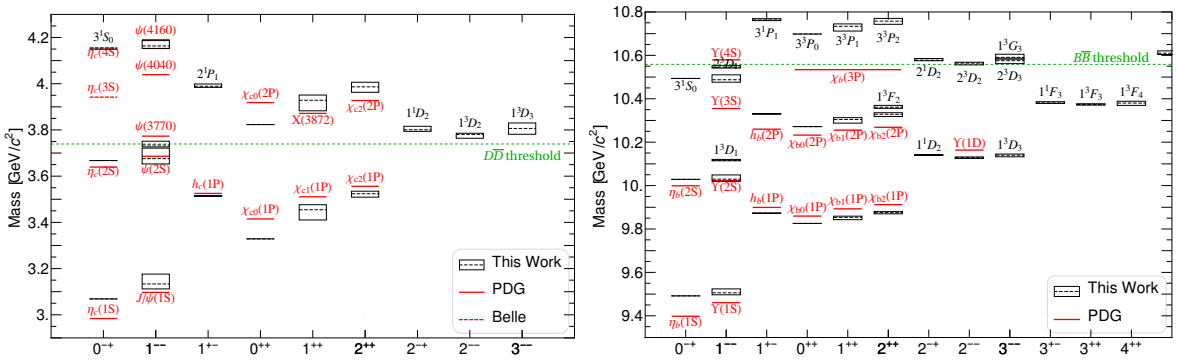

Figure 1: *Left*: the charmonium spectrum in GeV; *Right*: the bottomonium spectrum in GeV. The horizontal axes is J^{PC}. The known states are labeled by their PDG symbols. The unknown states are labeled by the non-relativistic symbols. The spread of M_{m_J} is indicated by a box and $\overline{M}$ is shown in dashed lines. Model parameters for our spectra shown here are given in Table 1 ($N_{\max} = L_{\max} = 24$).

Figure 1 shows the charmonium and bottomonium spectrum for $N_{\max} = L_{\max} = 24$. As mentioned, the mass degeneracy for m_J is lifted due to the violation of the rotational symmetry by the Fock sector truncation. We use a box to indicate the spread of masses M_{m_J} from different m_J. The r.m.s. values $\overline{M} = [(M_{-J}^2 + M_{1-J}^2 + \cdots + M_{+J}^2)/(2J+1)]^{\frac{1}{2}}$ are shown as dashed bars [51]. We compare our results with the experimental data from the particle data group (PDG, [60], cf. [61]). The r.m.s. deviations are computed for charmonium (bottomonium) below the $D\overline{D}$ ($B\overline{B}$) threshold (see Table. 1). Comparing with the recent results in Ref. [43], our approach improves the charmonium and bottomonium mass spectra from light-front holography.

The LFWFs can be used to calculate the transition amplitudes. Here we consider the decay constants. These quantities are useful for computing the decay widths and constraining the Standard Model parameters. In the non-relativistic limit, they are proportional to the wavefunctions at the origin and, therefore, test the short-distance physics of the model. The decay constants for a scalar S, a pseudo-scalar P, a axial-vector A, and a vector V states are defined as,

$$\begin{aligned} \langle 0|\overline{\psi}\gamma^\mu\gamma^5\psi|P(p)\rangle &= ip^\mu f_P, & \langle 0|\overline{\psi}\gamma^\mu\psi|V(p,\lambda)\rangle &= e_\lambda^\mu(p) m_V f_V\,, \quad (\lambda = 0, \pm 1) \\ \langle 0|\overline{\psi}\gamma^\mu\psi|S(p)\rangle &= p^\mu f_S, & \langle 0|\overline{\psi}\gamma^\mu\gamma^5\psi|A(p,\lambda)\rangle &= e_\lambda^\mu(p) m_A f_A\,, \quad (\lambda = 0, \pm 1) \end{aligned} \tag{20}$$

respectively, where $e_\lambda^\mu(p)$ is the spin vector for the vector boson,

$$e_\lambda(p) = (e_\lambda^+(p), e_\lambda^-(p), \boldsymbol{e}_\lambda^\perp(p)) = \begin{cases} \left(\frac{p^+}{m}, \frac{\boldsymbol{p}_\perp^2 - m^2}{mp^+}, \frac{\boldsymbol{p}^\perp}{m}\right), & \lambda = 0 \\ \left(0, \frac{2\boldsymbol{\epsilon}_\lambda^\perp \cdot \boldsymbol{p}^\perp}{p^+}, \boldsymbol{\epsilon}_\lambda^\perp\right), & \lambda = \pm 1. \end{cases} \tag{21}$$

Here $\boldsymbol{\epsilon}_\pm^\perp = (1, \pm i)/\sqrt{2}$. Note that due to the charge conjugation symmetry, the decay constants of 0^{++} and 1^{+-} vanish. In LFD, the decay constants can be computed from the "+" component of the current

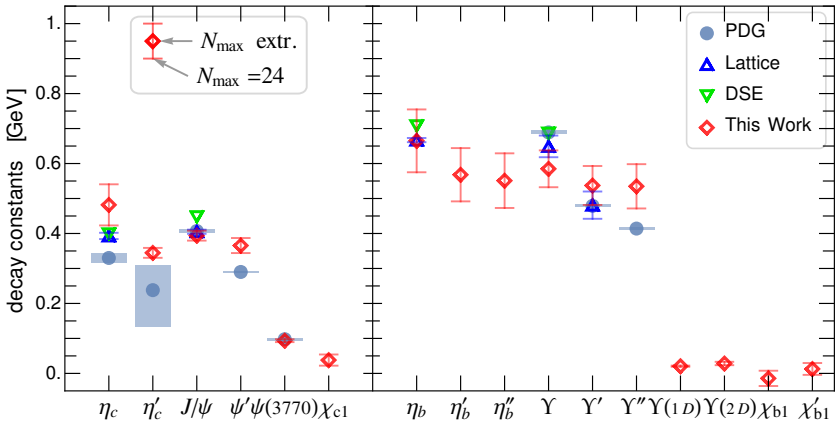

Figure 2: The decay constants of scalar and vector quarkonia as compared with PDG data [60] as well as Lattice QCD (Lattice) [62–65] and Dyson-Schwinger (DSE) [32] approaches. We extrapolate $N_{\max}$ using second-order polynomials in $N_{\max}^{-1}$ and adopt the difference between the extrapolated value ($N_{\max}$ extr.) and the $N_{\max} = 24$ value as the uncertainty (not including systematic errors). Note that $\Upsilon(nD)$ are referring to the vector bottomonia $\Upsilon(n^3D_1)$.

matrix elements, which read [10],

$$\begin{aligned} f_{P,A} =& 2\sqrt{N_c}\int_0^1 \frac{\mathrm{d}x}{2\sqrt{x(1-x)}}\int \frac{\mathrm{d}^2k_\perp}{(2\pi)^3}\left[\psi^J_{m_J=0}(\boldsymbol{k}_\perp,x,\uparrow,\downarrow) - \psi^J_{m_J=0}(\boldsymbol{k}_\perp,x,\downarrow,\uparrow)\right], \\ f_{S,V} =& 2\sqrt{N_c}\int_0^1 \frac{\mathrm{d}x}{2\sqrt{x(1-x)}}\int \frac{\mathrm{d}^2k_\perp}{(2\pi)^3}\left[\psi^J_{m_J=0}(\boldsymbol{k}_\perp,x,\uparrow,\downarrow) + \psi^J_{m_J=0}(\boldsymbol{k}_\perp,x,\downarrow,\uparrow)\right]. \end{aligned} \tag{22}$$

The decay constants from this work are plotted in Fig. 2. We also list the PDG data [60], as well as results from Lattice QCD (Lattice, [62–65]), and the Dyson-Schwinger equation (DSE, [32]). The PDG data are extracted from the dilepton decay widths Γ_{ee} (for vectors) and diphoton decay widths $\Gamma_{\gamma\gamma}$ (for pseudo-scalars). We obtain results for three successive sets of basis regulators, $N_{\max} = L_{\max} = 8, 16, 24$, where the parameters κ and m_q are fitted to the mass spectrum separately, and α_s, μ_g are kept fixed. We then extrapolate $N_{\max}$ using simply polynomials in $N_{\max}^{-1}$ and estimate the uncertainty associated with $N_{\max}$ from the difference between the extrapolated and the $N_{\max} = 24$ results. While the resultant masses are close as we mentioned, the decay constants show noticeable residual regulator dependence. This may not be a surprise as the decay constant probes the short-distance physics, whereas the basis is chosen to emulate confinement. We expect slower convergence for the decay constants than the masses.

From Fig. 2, our calculated decay constants are in reasonable agreement with the known experimental measurements as well as Lattice and DSE results. This is encouraging since the measured decay constants are not used in our fits. However, compared to Lattice and DSE results, most of our results are systematically larger than the PDG data. This is likely due to the systematic errors of our model and can be improved by more realistic models for the LF Hamiltonian and/or by including higher Fock spaces. Fig. 2 also includes decay constants for the D-wave states. In the non-relativistic limit, these quantities should vanish. The small but non-vanishing D-wave decay constants in our results indicate the mixing of the S-wave component, as expected from the relativistic treatment.

The LFWFs also provide direct access to other hadronic observables. Here we study the fictitious charge form factor with the photon coupling only to the quark (but not the anti-quark). Of course, this quantity is not a physical observable. Nevertheless, it provides important insight to the system. In particular, this charge form factor at small momentum transfer yields the r.m.s. radius of the hadron,

$$\langle r_h^2\rangle = -6\frac{\partial}{\partial Q^2}G_0(Q^2)\Big|_{Q\to 0.} \tag{23}$$

In LFD within the impulse approximation, the form factors can be obtained from the Drell-Yan-West

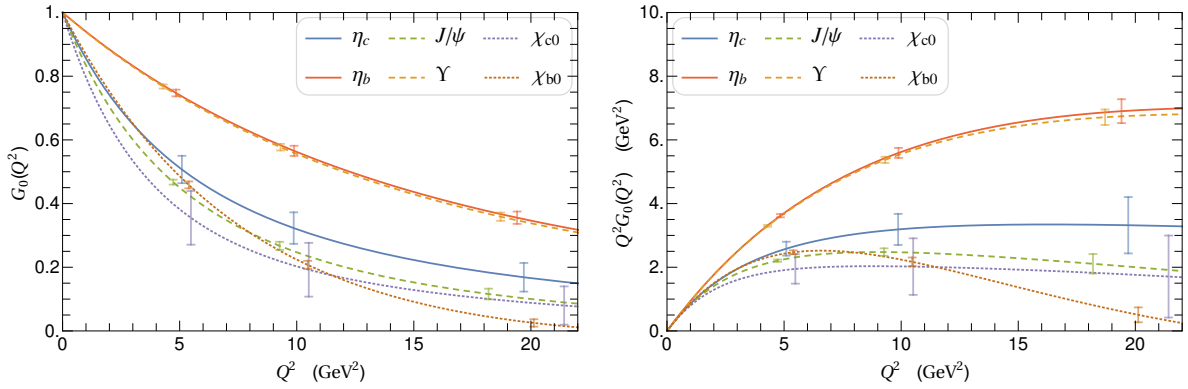

Figure 3: The charge form factors $G_0(Q^2)$ for η_c, J/ψ, χ_{c0}, η_b, Υ, and χ_{b0} as extrapolated from $N_{\max} = L_{\max} = 8, 16, 24$ using second-order polynomials in $N_{\max}^{-1}$. The difference between the extrapolated and the $N_{\max} = 24$ values are used to quantify the uncertainty, which does not include systematic errors. Note that, for the scales we are showing, the charge form factor of η_b and Υ are on top of each other.

Table 2: The mean squared radii (in fm^2) of charmonia and bottomonia as extrapolated from $N_{\max} = L_{\max} = 8, 16, 24$ using second-order polynomials in $N_{\max}^{-1}$. The difference between the extrapolated and the $N_{\max} = 24$ values are presented as the uncertainty, which does not include systematic errors.

(fm^2)	$\langle r^2_{\eta_c}\rangle$	$\langle r^2_{J/\psi}\rangle$	$\langle r^2_{\chi_{c0}}\rangle$	$\langle r^2_{\eta'_c}\rangle$	$\langle r^2_{\eta_b}\rangle$	$\langle r^2_{\Upsilon}\rangle$	$\langle r^2_{\chi_{b0}}\rangle$	$\langle r^2_{\eta'_b}\rangle$
this work	0.038(5)	0.0441(8)	0.06(1)	0.1488(5)	0.0146(8)	0.0149(5)	0.0331(8)	0.0510(8)
Lattice [70]	0.063(1)	0.066(2)	0.095(6)					
DSE [71]	0.048(4)	0.052(3)						

formula within the Drell-Yan frame $P'^+ = P^+$ [66],

$$\begin{aligned} I_{m_J,m'_J}(Q^2) &\triangleq \langle \psi^{J^{PC}}_{m'_J}(P')|J^+|\psi^{J^{PC}}_{m_J}(P)\rangle/(2P^+) \\ &= \sum_{s,\bar{s}} \int_0^1 \frac{\mathrm{d}x}{2x(1-x)} \int \frac{\mathrm{d}^2 k_\perp}{(2\pi)^3} \psi^{J*}_{m'_J}(\boldsymbol{k}_\perp + (1-x)\boldsymbol{q}_\perp, x, s, \bar{s}) \psi^{J}_{m_J}(\boldsymbol{k}_\perp, x, s, \bar{s}) \end{aligned} \tag{24}$$

where $q = P' - P$, and $Q^2 = -q^2 = \boldsymbol{q}_\perp^2$. For (pseudo) scalars, it directly produces the charge form factor $G_0(Q^2) = I_{0,0}(Q^2)$. For (axial) vector mesons, due to the violation of the rotational symmetry, there exists some ambiguity on finding the physical (Sachs) form factors G_0, G_1, and G_2 from I_{m_J,m'_J} [67]. We adopt the prescription of Grach and Kondratyuk [67], which has been shown to be free of zero-mode contributions in some analytical models [68, 69]. The charge form factor according to this prescription reads,

$$G_0 = \frac{1}{3}\left[(3-2\eta)I_{1,1} + 2\sqrt{2\eta} I_{1,0} + I_{1,-1}\right], \tag{25}$$

where $\eta = Q^2/(4M^2)$, M is the mass of the hadron. Fig. 3 shows the charge form factors of η_c, J/ψ, χ_{c0}, η_b, Υ, and χ_{b0}. Table 2 lists the r.m.s. radii of the first few states. From our results, the radius of J/ψ is close to, but slightly larger than, that of η_c. This is consistent with the Lattice and DSE results and can be understood from the non-relativistic point of view. Bottomonia are in general smaller than charmonia, a result, again, that can be drawn from the non-relativistic argument. The comparison of the first few available results shows that radii from our approach are in qualitative agreement with those of other approaches [70, 71], though ours are systematically smaller than the Lattice and DSE results. This observation is consistent with the trend of the decay constants.

5. Summary and Outlook

We studied heavy quarkonium based on holographic QCD and a realistic one-gluon exchange on the light front. We proposed a longitudinal confining potential to incorporate quark mass and longitudinal dynamics. We solved the bound-state problem in the Basis Light-Front Quantization approach. We calculated the spectroscopy, decay constants and charge form factors for the charmonium and bottomonium. The comparison with the experimental data and results from Lattice QCD and Dyson-Schwinger equation shows reasonable agreement among the available observables. As such, we improve the light-front holography from the first approximation to QCD.

The LFWFs may readily be used in the study of, e.g., radiative transitions [26] and diffractive vector meson production in ultra-peripheral heavy ion collisions [72]. These observables will also serve as stringent tests of our model in different regimes.

This model can also be applied to heavy-light and light-light systems, where the light-front holography provides a good initial approximation [45]. The phenomenological confinement can be improved by a better understanding of the string/gauge duality as well as a more complete derivation of the inter-quark potentials from various first-principle approaches to QCD [73]. Ultimately, the phenomenological confining interaction should be replaced by the QCD Hamiltonian.

This work can be extended to higher Fock sectors to incorporate sea-quark and gluon degrees of freedom as well. The treatment of the many-body dynamics is essential for obtaining realistic predictions for states above the thresholds. One of the major challenges of the light-front Hamiltonian approach however is that explicitly including many gluons, as well as many quark-antiquark pairs, in the Fock space expansion quickly becomes numerically expensive. The ever increasing computational capacity and the progress in *ab initio* many-body calculations represent growing opportunities for understanding the strong interaction in the Basis Light-Front Quantization approach. For systems involving light quarks, however, the naïve Fock sector truncation may not suffice, as addressing dynamical chiral symmetry breaking is essential [74]. The coherent basis (see, e.g., [75]) and the light-front coupled-cluster method [76] are two promising approaches for dealing with collective modes and dynamical symmetry breaking in the light-front Hamiltonian formalism.

Acknowledgements

We wish to thank P. Wiecki, V.A. Karmanov, S.J. Brodsky, G. de Téramond, A.P. Trawiński, S. Prell, J.R. Spence, A.M. Shirokov, S.D. Głazek and G. Chen for valuable discussions. We thank G. Chen for cross-checking the expressions and the codes. This work was supported in part by the Department of Energy under Grant Nos. DE-FG02-87ER40371 and DESC0008485 (SciDAC-3/NUCLEI) and by the National Science Foundation under Grant No. PHY-0904782. X. Zhao is supported by the new faculty startup funding by the Institute of Modern Physics, Chinese Academy of Sciences under Grant No. Y532070ZY0.

References

[1] J.M. Maldacena, Adv. Theor. Math. Phys. **2**, 231 (1998); [arXiv:hep-th/9711200].
[2] A. Karch, E. Katz, D.T. Son and M.A. Stephanov, Phys. Rev. D **74**, 015005 (2006); [arXiv:hep-ph/0602229].
[3] Y. Kim, I.J. Shin, T. Tsukioka, Prog. Part. Nucl. Phys. **68**, 55 (2013); [arXiv:1205.4852 [hep-ph]].
[4] P. Maris, M. Sosonkina, J.P. Vary, E. Ng and C. Yang, Procedia Comput. Science **1**, 97 (2010).
[5] B.R. Barrett, P. Navrátil, J.P. Vary, Prog. Part. Nucl. Phys. **69**, 131 (2013).
[6] H.M. Aktulga, C. Yang, E.G. Ng, P. Maris and J.P. Vary, Concurrency Computat.: Pract. Exper. **26**, 2631 (2013).
[7] M.A. Caprio, P. Maris, J.P. Vary and R. Smith, Int. J. Mod. Phys. E **24**, 1541002 (2015).
[8] J.P. Vary, H. Honkanen, Jun Li, P. Maris, S.J. Brodsky, A. Harindranath, G.F. de Teramond, P. Sternberg, E.G. Ng, and C. Yang, Phys. Rev. C **81**, 035205 (2010); [arXiv:0812.1819 [nucl-th]].
[9] B.L.G. Bakker *et al.*, Nucl. Phys. Proc. Suppl. **251-252**, 165 (2014); [arXiv:1309.6333 [hep-ph]].
[10] G.P. Lepage, and S.J. Brodsky, Phys. Rev. D **22**, 2157 (1980).
[11] S.J. Brodsky, M. Diehl, D.S. Hwang, Nucl. Phys. B **596**, 99 (2001); [arXiv:hep-ph/0009254].
[12] S.J. Brodsky, H.-C. Pauli and S. Pinsky, Phys. Rept. **301**, 299 (1998); [arXiv:hep-ph/9705477].
[13] Yang Li, P.W. Wiecki, X. Zhao, P. Maris and J.P. Vary, Proc. Int. Conf. Nucl. Theor. Supercomputing Era (NTSE-2013), Eds. A.M. Schirokov and A.I. Mazur. Pacific National University, Khabarovsk, 2014.
[14] P. Maris, P. Wiecki, Yang Li, X. Zhao and J.P. Vary, Acta Phys. Polon. Supp., **6**, 321 (2013).

[15] J.P. Vary, P. Maris, E. Ng, C. Yang and M. Sosonkina, J. Phys. Conf. Ser. **180**, 012083 (2009).
[16] H. Honkanen, P. Maris, J.P. Vary and S.J. Brodsky, Phys. Rev. Lett. **106**, 061603 (2011); [arXiv:1008.0068 [hep-ph]].
[17] X. Zhao, H. Honkanen, P. Maris, J.P. Vary, S.J. Brodsky, Phys. Lett. B **737**, 65-69 (2014); [arXiv:1402.4195 [nucl-th]].
[18] X. Zhao, A. Ilderton, P. Maris and J. P. Vary, Phys. Lett. B **726**, 856 (2013); [arXiv:1309.5338 [nucl-th]].
[19] X. Zhao, A. Ilderton, P. Maris, J.P. Vary, Phys. Rev. D **88**, 065014 (2013); [arXiv:1303.3273 [nucl-th]].
[20] P. Wiecki, Yang Li, X. Zhao, P. Maris, J.P. Vary, Phys. Rev. D **91**, 105009 (2015); [arXiv:1404.6234 [nucl-th]].
[21] J.P. Vary, P. Wiecki, Yang Li, X. Zhao, P. Maris, Manuscript in preparation.
[22] M. Kaluza and H.C. Pauli, Phys. Rev. D **45**, 2968 (1992).
[23] M. Krautgartner, H.-C. Pauli and F. Wolz, Phys. Rev. D **45**, 3755 (1992).
[24] U. Trittmann and H.-C. Pauli, MPI H-V4-1997; [hep-th/9704215].
[25] H. Lamm and R.F. Lebed, J. Phys. G **41**, 125003 (2014); [arXiv:1311.3245 [hep-ph]].
[26] N. Brambilla, *et al.*, Eur. Phys. J. C **71**, 1534 (2011); [arXiv:1010.5827 [hep-ph]].
[27] T. Applelquist, R. M. Barnett, K. Lane, Ann. Rev. Nucl. Part. Sci. **28**, 387 (1978).
[28] S. Godfrey and N. Isqur, Phys. Rev. D **32**, 189 (1985).
[29] N. Brambilla, A. Pineda, J. Soto, and A. Vairo, Rev. Mod. Phys. **77**, 1423 (2005); [arXiv:hep-ph/0410047].
[30] M. Neubert, Phys. Rept. **245**, 259 (1994); [arXiv:hep-ph/9306320].
[31] M.S. Bhagwat, P. Maris, Phys. Rev. C **77**, 025203 (2008); [arXiv:nucl-th/0612069].
[32] M. Blank and A. Krassnigg. Phys. Rev. D **84**, 096014 (2011); [arXiv:1109.6509 [hep-ph]].
[33] T. Hilger, C. Popovici, M. Gomez-Rocha and A. Krassnigg, Phys. Rev. D **91**, 034013 (2015); [arXiv:1409.3205 [hep-ph]].
[34] C.S. Fischer, S. Kubrak, R. Williams, Eur. Phys. J. A **51**, 10 (2015); [arXiv:1409.5076 [hep-ph]].
[35] C. McNeile, Lect. Notes Phys. **647**, 100 (2004); [hep-lat/0210026].
[36] M. Ablikim *et al.* (BESIII Collaboration), Phys. Rev. Lett. **110**, 252001 (2013); [arXiv:1303.5949 [hep-ex]]. Z.Q. Liu *et al.* (Belle Collaboration), *ibid.* **110**, 252002 (2013); [arXiv:1304.0121 [hep-ex]]. Erratum: *ibid.* **111**, 019901 (2013).
[37] R. Aaij *et al.* (LHCb collaboration), [arXiv:1507.03414 [hep-ex]].
[38] N.N. Singh, Y.K. Mathur and A.N. Mitra, Few-Body Syst. **1**, 47-62 (1986).
[39] M.M. Brisudova and R. Perry, Phys. Rev. D **54**, 1831 (1996); [hep-ph/9511443].
[40] M.M. Brisudova, R.J. Perry, KG. Wilson, Phys. Rev. Lett. **78**, 1227 (1997); [hep-ph/9607280].
[41] S.D. Głazek and J. Młynik, Phys. Rev. D **74**, 105015 (2006); [arXiv:hep-th/0606235v2].
[42] T. Branz, T. Gutsche, V.E. Lyubovitskij, I. Schmidt, A. Vega, Phys. Rev. D **82**, 074022 (2010); [arXiv:1008.0268].
[43] T. Gutsche, V.E. Lyubovitskij, I. Schmidt, A. Vega, Phys. Rev. D **90**, 096007 (2014); [arXiv:1410.3738].
[44] H.-M. Choi, Phys. Rev. D **75**, 073016 (2007); [arXiv:hep-ph/0701263].
[45] S.J. Brodsky, G.F. de Teramond, H.G. Dosch, J. Erlich, Phys. Rept. **584**, 1 (2015); [arXiv:1407.8131 [hep-ph]].
[46] G.F. de Teramond, S.J. Brodsky, Phys. Rev. Lett. **102**, 081601 (2009); [arXiv:0809.4899 [hep-ph]].
[47] S.D. Głazek, Acta Phys. Polon. **B42**, 1933 (2011).
[48] A.P. Trawiński, S.D. Głazek, S.J. Brodsky, G.F. de Téramond, H.G. Dosch, Phys. Rev. D **90**, 074017 (2014); [arXiv:1403.5651v1 [hep-ph]].
[49] S.S. Chabysheva, and J.R. Hiller, Ann. of Phys. **337**, 143-152 (2013); [arXiv:1207.7128 [hep-ph]].
[50] F. Antonuccio, S.J. Brodsky, and S. Dalley. Phys. Lett. B **412**, 104 (1997); [arXiv:hep-ph/9705413].
[51] M. Mangin-Brinet, J. Carbonell, V.A. Karmanov, Phys. Rev. C **68**, 055203 (2003); [hep-th/0308179].
[52] R.J. Perry and A. Harindranath, Phys. Rev. D **43**, 4051 (1991).
[53] S. Głazek, A. Harindranath, S. Pinsky, J. Shigemitsu and K.G. Wilson, Phys. Rev. D **47**, 1599 (1993).
[54] S.D. Głazek and K.G. Wilson, Phys. Rev. D **48**, 5863 (1993).
[55] J.R. Hiller and S.J. Brodsky, Phys. Rev. D **59**, 016006 (1998); [arXiv:hep-ph/9806541].
[56] V.A. Karmanov, J.-F Mathiot, A.V. Smirnov, Phys. Rev. D **77**, 085028 (2008); [arXiv:0801.4507 [hep-th]].
[57] S.A. Coon, M.I. Avetian, M.K.G. Kruse, U. van Kolck, P. Maris and J.P. Vary, Phys. Rev. C **86**, 054002 (2012); [arXiv:1205.3230 [nucl-th]].
[58] D.E. Soper, Phys. Rev. D **5**, 1956 (1972).
[59] E. Anderson *et al.*, "LAPACK Users' Guide", 3rd Eds., Society for Industrial and Applied Mathematics, Philadelphia, PA, 1999.
[60] K.A. Olive *et al.* (Particle Data Group), Chin. Phys. C38, 090001 (2014), [`http://pdg.lbl.gov`].
[61] A.J. Bevan *et al.* (Belle Collaboration), Eur. Phy. J. C **74**, 3026 (2014); [arXiv:1406.6311 [hep-ex]].
[62] C.T.H. Davies, C. McNeile, E. Follana, G.P. Lepage, H. Na, J. Shigemitsu (HPQCD Collaboration), Phys. Rev. D **82**, 114504 (2010); [arXiv:1008.4018 [hep-lat]].
[63] C. McNeile, C.T.H. Davies, E. Follana, K. Hornbostel, G.P. Lepage (HPQCD Collaboration), Phys. Rev. D **86**, 074503 (2012); [arXiv:1207.0994 [hep-lat]].
[64] G.C. Donald, C.T.H. Davies, R.J. Dowdall, E. Follana, K. Hornbostel, J. Koponen, G.P. Lepage, C. McNeile (HPQCD Collaboration), Phys. Rev. D **86**, 094501 (2012); [arXiv:1208.2855 [hep-lat]].
[65] B. Colquhoun, R.J. Dowdall, C.T.H. Davies, K. Hornbostel, G.P. Lepage (HPQCD Collaboration), Phys. Rev. D **91**, 074514 (2015); [arXiv:1408.5768 [hep-lat]].
[66] S.D. Drell and T.M. Yan, Phys. Rev. Lett. **24**, 181 (1970); G.B. West, *ibid.* **24**, 1206 (1970).
[67] I.L. Grach and L.A. Kondratyuk, Sov. J. Nucl. Phys. **39**, 198 (1984).
[68] V.A. Karmanov, Nucl. Phys. A **608**, 316 (1996).
[69] J.P.B.C. de Melo and T. Frederico, Phys. Rev. C **55**, 2043 (1997); [arXiv:nucl-th/9706032v3].
[70] J.J. Dudek, R.G. Edwards and D.G. Richards, Phys. Rev. D **73**, 074507 (2006); [arXiv:hep-ph/0601137].
[71] P. Maris, AIP Conf. Proc. **892**, 65–71 (2007); [arXiv:nucl-th/0611057].
[72] A. Baltz et. al., Phys. Rept. **458**, 1 (2008); [arXiv:0706.3356 [nucl-ex]].
[73] A.V. Smirnov, V.A. Smirnov, and M. Steinhauser, Phys. Rev. Lett. **104**, 112002 (2010).
[74] K. Itakura, and S. Maedan, Phys. Rev. D **61**, 045009 (2000); *ibid*: **62**, 105016 (2000).
[75] A. Misra, Phys. Rev. D **62**, 125017 (2000).
[76] S.S. Chabysheva and J.R. Hiller, Phys. Lett. B **711**, 417 (2012).

Supplementary data for "quarkonium in a holographic basis"

Yang Li, Pieter Maris, Xingbo Zhao, and James P. Vary

April 5, 2016

Table 1: Summary of the model parameters. The coupling α_s and the gluon mass μ_g are fixed. We choose the bottomonium $\alpha_s(9.5\,\mathrm{GeV}) = 0.25$ and then obtain the charmonium coupling $\alpha_s(3.5\,\mathrm{GeV}) \simeq 0.36$ from pQCD evolution of the strong coupling. The confining strength κ and the quark mass m_q ($m_q = m_{\bar{q}}$) are fitted with $m_J = 0$ using the experimental data below the $D\overline{D}$ or $B\overline{B}$ threshold. The r.m.s. deviations for the $m_J = 0$ spectrum, $\delta M_{m_J=0}$, and the r.m.s. average-m_J spectrum, $\delta\overline{M}$, are computed for states below the threshold. The numbers for κ, m_q, $\delta M_{m_J=0}$ and $\delta\overline{M}$ are rounded.

No.		α_s	μ_g (GeV)	κ (GeV)	m_q (GeV)	$\delta M_{m_J=0}$ (MeV)	$\delta\overline{M}$ (MeV)	$N_{\max} = L_{\max}$
I	$c\bar{c}$	0.3595	0.02	0.963	1.492	65 (8 states)	56 (8 states)	8
	$b\bar{b}$	0.2500		1.492	4.758	59 (14 states)	55 (14 states)	
II	$c\bar{c}$	0.3595	0.02	0.950	1.510	64 (8 states)	52 (8 states)	16
	$b\bar{b}$	0.2500		1.491	4.761	56 (14 states)	51 (14 states)	
III	$c\bar{c}$	0.3595	0.02	0.938	1.522	65 (8 states)	52 (8 states)	24
	$b\bar{b}$	0.2500		1.490	4.763	54 (14 states)	50 (14 states)	

Table 2: The charmonium spectrum and decay constants ($N_{\max} = L_{\max} = 8, \kappa = 0.963\,\mathrm{GeV}, m_c = 1.492\,\mathrm{GeV}$). M_{pdg} quotes charmonium masses from Particle Data Group[1] (PDG 2014). $M_{m_J=0}$ collects the masses from the $m_J = 0$ sector. The r.m.s. average-m_J mass $\overline{M} = \left[(M_{-J}^2 + M_{1-J}^2 + \cdots + M_{+J}^2)/(2J+1)\right]^{\frac{1}{2}}$. $M_{\min} = \min\{M_{m_J}\}$, $M_{\max} = \max\{M_{m_J}\}$.

	$n\,^{2S+1}L_J$	J^{PC}	M_{pdg}(GeV)	$M_{m_J=0}$(GeV)	$\overline{M}$(GeV)	$M_{\min}$(GeV)	$M_{\max}$(GeV)	f (GeV)
$\eta_c(1S)^*$	$1\,^1S_0$	0^{-+}	2.9836	3.07979	3.07979	3.07979	3.07979	0.36081
$J/\psi(1S)^*$	$1\,^3S_1$	1^{--}	3.096916	3.14431	3.10975	3.09233	3.14431	0.35066
$\chi_{c0}(1P)^*$	$1\,^3P_0$	0^{++}	3.41475	3.35285	3.35285	3.35285	3.35285	0.
$\chi_{c1}(1P)^*$	$1\,^3P_1$	1^{++}	3.51066	3.40689	3.44322	3.40689	3.46125	0.06155
$h_c(1P)^*$	$1\,^1P_1$	1^{+-}	3.52538	3.49972	3.49546	3.49333	3.49972	0.
$\chi_{c2}(1P)^*$	$1\,^3P_2$	2^{++}	3.5562	3.51397	3.50420	3.48788	3.51557	
$\eta_c(2S)^*$	$2\,^1S_0$	0^{-+}	3.6394	3.69728	3.69728	3.69728	3.69728	0.29471
$\psi(2S)^*$	$2\,^3S_1$	1^{--}	3.686109	3.72362	3.68679	3.66824	3.72362	0.30062
$\psi(3770)$	$1\,^3D_1$	1^{--}	3.77315	3.74542	3.72814	3.71946	3.74542	0.07773
	$1\,^3D_2$	2^{--}		3.75804	3.77571	3.75804	3.78275	
	$1\,^1D_2$	2^{-+}		3.81879	3.79676	3.78678	3.81879	
	$1\,^3D_3$	3^{--}		3.83039	3.80230	3.77322	3.83039	
$\chi_{c0}(2P)$	$2\,^3P_0$	0^{++}	3.9184	3.88304	3.88304	3.88304	3.88304	0.
$X(3872)$	$2\,^3P_1$	1^{++}	3.87169	3.91125	3.95026	3.91125	3.96962	0.07521
$X(3900)^{\pm}$	$2\,^1P_1$	1^{+-}	3.8887	4.01287	4.00042	3.99419	4.01287	0.
$\chi_{c2}(2P)$	$2\,^3P_2$	2^{++}	3.9272	4.01768	3.99424	3.96949	4.01768	
	$3\,^1S_0$	0^{-+}		4.20176	4.20176	4.20176	4.20176	0.25915
$\psi(4040)$	$3\,^3S_1$	1^{--}	4.039	4.21367	4.17769	4.15958	4.21367	0.26696

* States whose masses are used to fit the parameters κ and m_c in this work.

[1] K.A. Olive et al. (Particle Data Group), Chin. Phys. C **38**, 090001 (2014); [http://pdg.lbl.gov].

Table 3: The charmonium spectrum and decay constants ($N_{\max} = L_{\max} = 16, \kappa = 0.950\,\mathrm{GeV}, m_c = 1.510\,\mathrm{GeV}$). M_{pdg} quotes charmonium masses from Particle Data Group[1] (PDG 2014). $M_{m_J=0}$ collects the masses from the $m_J = 0$ sector. The r.m.s. average-m_J mass $\overline{M} = \left[(M_{-J}^2 + M_{1-J}^2 + \cdots + M_{+J}^2)/(2J+1)\right]^{\frac{1}{2}}$. $M_{\min} = \min\{M_{m_J}\}$, $M_{\max} = \max\{M_{m_J}\}$.

	$n\,^{2S+1}L_J$	J^{PC}	M_{pdg}(GeV)	$M_{m_J=0}$(GeV)	$\overline{M}$(GeV)	$M_{\min}$(GeV)	$M_{\max}$(GeV)	f (GeV)
$\eta_c(1S)^*$	$1\,^1S_0$	0^{-+}	2.9836	3.07306	3.07306	3.07306	3.07306	0.40055
$J/\psi(1S)^*$	$1\,^3S_1$	1^{--}	3.096916	3.16284	3.12261	3.10230	3.16284	0.37249

$\chi_{c0}(1P)^*$	$1\,^3P_0$	0^{++}	3.41475	3.33761	3.33761	3.33761	3.33761	0.
$\chi_{c1}(1P)^*$	$1\,^3P_1$	1^{++}	3.51066	3.40861	3.44986	3.40861	3.47030	0.05899
$h_c(1P)^*$	$1\,^1P_1$	1^{+-}	3.52538	3.51013	3.50708	3.50555	3.51013	0.
$\chi_{c2}(1P)^*$	$1\,^3P_2$	2^{++}	3.5562	3.52568	3.51702	3.50142	3.52823	
$\eta_c(2S)^*$	$2\,^1S_0$	0^{-+}	3.6394	3.67956	3.67956	3.67956	3.67956	0.32243
$\psi(2S)^*$	$2\,^3S_1$	1^{--}	3.686109	3.72234	3.67897	3.65710	3.72234	0.33323
$\psi(3770)$	$1\,^3D_1$	1^{--}	3.77315	3.74999	3.73280	3.72418	3.74999	0.08694
	$1\,^3D_2$	2^{--}		3.76292	3.78028	3.76292	3.78602	
	$1\,^1D_2$	2^{-+}		3.81867	3.80099	3.79281	3.81867	
	$1\,^3D_3$	3^{--}		3.83233	3.80674	3.77982	3.83233	
$\chi_{c0}(2P)$	$2\,^3P_0$	0^{++}	3.9184	3.84589	3.84589	3.84589	3.84589	0.
$X(3872)$	$2\,^3P_1$	1^{++}	3.87169	3.89320	3.93699	3.89320	3.95870	0.09212
$X(3900)^{\pm}$	$2\,^1P_1$	1^{+-}	3.8887	4.00585	3.99503	3.98960	4.00585	0.
$\chi_{c2}(2P)$	$2\,^3P_2$	2^{++}	3.9272	4.01273	3.99120	3.96669	4.01273	
	$3\,^1S_0$	0^{-+}		4.17128	4.17128	4.17128	4.17128	0.29910
$\psi(4040)$	$3\,^3S_1$	1^{--}	4.039	4.19738	4.15054	4.12692	4.19738	0.28728

* States whose masses are used to fit the parameters κ and m_c in this work.

[1] K.A. Olive et al. (Particle Data Group), Chin. Phys. C **38**, 090001 (2014); [http://pdg.lbl.gov].

Table 4: The charmonium spectrum and decay constants ($N_{\max} = L_{\max} = 24, \kappa = 0.938\,\text{GeV}, m_c = 1.522\,\text{GeV}$). M_{pdg} quotes charmonium masses from Particle Data Group[1] (PDG 2014). $M_{m_J=0}$ collects the masses from the $m_J = 0$ sector. The r.m.s. average-m_J mass $\overline{M} = \left[(M_{-J}^2 + M_{1-J}^2 + \cdots + M_{+J}^2)/(2J+1)\right]^{\frac{1}{2}}$. $M_{\min} = \min\{M_{m_J}\}$, $M_{\max} = \max\{M_{m_J}\}$.

	$n\,^{2S+1}L_J$	J^{PC}	M_{pdg}(GeV)	$M_{m_J=0}$(GeV)	$\overline{M}$(GeV)	$M_{\min}$(GeV)	$M_{\max}$(GeV)	f (GeV)
$\eta_c(1S)^*$	$1\,^1S_0$	0^{-+}	2.9836	3.06877	3.06877	3.06877	3.06877	0.42302
$J/\psi(1S)^*$	$1\,^3S_1$	1^{--}	3.096916	3.17612	3.13355	3.11205	3.17612	0.37965
$\chi_{c0}(1P)^*$	$1\,^3P_0$	0^{++}	3.41475	3.32860	3.32860	3.32860	3.32860	0.
$\chi_{c1}(1P)^*$	$1\,^3P_1$	1^{++}	3.51066	3.41041	3.45460	3.41041	3.47649	0.05406
$h_c(1P)^*$	$1\,^1P_1$	1^{+-}	3.52538	3.51612	3.51375	3.51256	3.51612	0.
$\chi_{c2}(1P)^*$	$1\,^3P_2$	2^{++}	3.5562	3.53182	3.52396	3.50908	3.53486	
$\eta_c(2S)^*$	$2\,^1S_0$	0^{-+}	3.6394	3.66753	3.66753	3.66753	3.66753	0.33044
$\psi(2S)^*$	$2\,^3S_1$	1^{--}	3.686109	3.72126	3.67578	3.65283	3.72126	0.34403
$\psi(3770)$	$1\,^3D_1$	1^{--}	3.77315	3.75121	3.73492	3.72675	3.75121	0.08943
	$1\,^3D_2$	2^{--}		3.76390	3.78070	3.76390	3.78569	
	$1\,^1D_2$	2^{-+}		3.81578	3.80081	3.79382	3.81578	
	$1\,^3D_3$	3^{--}		3.83024	3.80650	3.78128	3.83024	
$\chi_{c0}(2P)$	$2\,^3P_0$	0^{++}	3.9184	3.82321	3.82321	3.82321	3.82321	0.
$X(3872)$	$2\,^3P_1$	1^{++}	3.87169	3.88279	3.92842	3.88279	3.95105	0.09723
$X(3900)^{\pm}$	$2\,^1P_1$	1^{+-}	3.8887	3.99890	3.98910	3.98419	3.99890	0.
$\chi_{c2}(2P)$	$2\,^3P_2$	2^{++}	3.9272	4.00641	3.98650	3.96288	4.00641	
	$3\,^1S_0$	0^{-+}		4.15002	4.15002	4.15002	4.15002	0.30702
$\psi(4040)$	$3\,^3S_1$	1^{--}	4.039	4.18663	4.16370	4.15218	4.18663	0.28008

* States whose masses are used to fit the parameters κ and m_c in this work.

[1] K.A. Olive et al. (Particle Data Group), Chin. Phys. C **38**, 090001 (2014); [http://pdg.lbl.gov].

Table 5: The bottomonium spectrum and decay constants ($N_{\max} = L_{\max} = 8, \kappa = 1.492\,\text{GeV}, m_b = 4.758\,\text{GeV}$). M_{pdg} quotes bottomonium masses from Particle Data Group[1] (PDG 2014). $M_{m_J=0}$ collects the masses from the $m_J = 0$ sector. The r.m.s. average-m_J mass $\overline{M} = \left[(M_{-J}^2 + M_{1-J}^2 + \cdots + M_{+J}^2)/(2J+1)\right]^{\frac{1}{2}}$. $M_{\min} = \min\{M_{m_J}\}$, $M_{\max} = \max\{M_{m_J}\}$.

	$n\,^{2S+1}L_J$	J^{PC}	M_{pdg}(GeV)	$M_{m_J=0}$(GeV)	$\overline{M}$(GeV)	$M_{\min}$(GeV)	$M_{\max}$(GeV)	f(GeV)
$\eta_b(1S)^*$	$1\,^1S_0$	0^{-+}	9.398	9.50231	9.50231	9.50231	9.50231	0.46979
$\Upsilon(1S)^*$	$1\,^3S_1$	1^{--}	9.4603	9.52295	9.50957	9.50288	9.52295	0.45714
$\chi_{b0}(1P)^*$	$1\,^3P_0$	0^{++}	9.85944	9.82548	9.82548	9.82548	9.82548	0.
$h_b(1P)^*$	$1\,^1P_1$	1^{+-}	9.8993	9.86487	9.86623	9.86487	9.86691	0.
$\chi_{b1}(1P)^*$	$1\,^3P_1$	1^{++}	9.89278	9.83976	9.84875	9.83976	9.85325	0.02550
$\chi_{b2}(1P)^*$	$1\,^3P_2$	2^{++}	9.91221	9.86946	9.86803	9.86272	9.87262	
$\eta_b(2S)^*$	$2\,^1S_0$	0^{-+}	9.999	10.04033	10.04033	10.04033	10.04033	0.39332
$\Upsilon(2S)^*$	$2\,^3S_1$	1^{--}	10.02326	10.05169	10.03727	10.03005	10.05169	0.39680

	$1\,^3D_1$	1^{--}		10.11386	10.11010	10.10822	10.11386	0.01723
$\Upsilon(1D)^*$	$1\,^3D_2$	2^{--}	10.1637	10.11785	10.12319	10.11785	10.12463	
	$1\,^1D_2$	2^{-+}		10.13580	10.13294	10.13177	10.13580	
	$1\,^3D_3$	3^{--}		10.13542	10.13272	10.12568	10.13597	
$\chi_{b0}(2P)^*$	$2\,^3P_0$	0^{++}	10.2325	10.28144	10.28144	10.28144	10.28144	0.
$h_b(2P)^*$	$2\,^1P_1$	1^{+-}	10.2598	10.32862	10.32696	10.32614	10.32862	0.
$\chi_{b1}(2P)^*$	$2\,^3P_1$	1^{++}	10.25546	10.29200	10.30551	10.29200	10.31226	0.03913
$\chi_{b2}(2P)^*$	$2\,^3P_2$	2^{++}	10.26865	10.33087	10.32467	10.31497	10.33127	
	$1\,^3F_2$	2^{++}		10.36309	10.35457	10.34957	10.36309	
	$1\,^3F_3$	3^{++}		10.36561	10.36731	10.36419	10.37097	
	$1\,^1F_3$	3^{+-}		10.38030	10.37436	10.37182	10.38030	
	$1\,^3F_4$	4^{++}		10.38223	10.37372	10.36290	10.38223	
	$3\,^1S_0$	0^{-+}		10.51184	10.51184	10.51184	10.51184	0.35815
$\Upsilon(3S)^*$	$3\,^3S_1$	1^{--}	10.3552	10.51945	10.50394	10.49617	10.51945	0.36402
	$2\,^3D_1$	1^{--}		10.54918	10.54435	10.54193	10.54918	0.02425
	$2\,^3D_2$	2^{--}		10.55200	10.56022	10.55200	10.56478	
	$2\,^1D_2$	2^{-+}		10.58138	10.57365	10.57153	10.58138	
	$2\,^3D_3$	3^{--}		10.58271	10.57122	10.55865	10.58271	
	$1\,^3G_3$	3^{--}		10.59956	10.58520	10.57695	10.59956	
	$1\,^3G_4$	4^{--}		10.60157	10.59853	10.58970	10.60684	
	$1\,^1G_4$	4^{-+}		10.61546	10.60405	10.59818	10.61546	
	$1\,^3G_5$	5^{--}		10.61732	10.60322	10.58792	10.61732	
$\chi_{b?}(3P)$	$3\,^3P_0$	0^{++}	10.5794	10.72027	10.72027	10.72027	10.72027	0.
	$3\,^3P_1$	1^{++}		10.72703	10.74293	10.72703	10.75087	0.04392
	$3\,^1P_1$	1^{+-}		10.77096	10.76538	10.76259	10.77096	0.
	$3\,^3P_2$	2^{++}		10.77131	10.75943	10.74662	10.77131	
	$4\,^1S_0$	0^{-+}		10.95999	10.95999	10.95999	10.95999	0.31175
$\Upsilon(4S)$	$4\,^3S_1$	1^{--}	10.5794	10.96411	10.95056	10.94377	10.96411	0.29659

* States whose masses are used to fit the parameters κ and m_b in this work.

[1] K.A. Olive et al. (Particle Data Group), Chin. Phys. C **38**, 090001 (2014); [`http://pdg.lbl.gov`].

Table 6: The bottomonium spectrum and decay constants ($N_{\max} = L_{\max} = 16, \kappa = 1.491\,\text{GeV}, m_b = 4.761\,\text{GeV}$). M_{pdg} quotes bottomonium masses from Particle Data Group[1] (PDG 2014). $M_{m_J=0}$ collects the masses from the $m_J = 0$ sector. The r.m.s. average-m_J mass $\overline{M} = \left[(M_{-J}^2 + M_{1-J}^2 + \cdots + M_{+J}^2)/(2J+1)\right]^{\frac{1}{2}}$. $M_{\min} = \min\{M_{m_J}\}$, $M_{\max} = \max\{M_{m_J}\}$.

	$n\,^{2S+1}L_J$	J^{PC}	M_{pdg}(GeV)	$M_{m_J=0}$(GeV)	$\overline{M}$(GeV)	$M_{\min}$(GeV)	$M_{\max}$(GeV)	f(GeV)
$\eta_b(1S)^*$	$1\,^1S_0$	0^{-+}	9.398	9.49520	9.49520	9.49520	9.49520	0.53938
$\Upsilon(1S)^*$	$1\,^3S_1$	1^{--}	9.4603	9.52317	9.50657	9.49826	9.52317	0.50967
$\chi_{b0}(1P)^*$	$1\,^3P_0$	0^{++}	9.85944	9.82577	9.82577	9.82577	9.82577	0.
$h_b(1P)^*$	$1\,^1P_1$	1^{+-}	9.8993	9.86971	9.87106	9.86971	9.87173	0.
$\chi_{b1}(1P)^*$	$1\,^3P_1$	1^{++}	9.89278	9.84213	9.85228	9.84213	9.85735	0.01536
$\chi_{b2}(1P)^*$	$1\,^3P_2$	2^{++}	9.91221	9.87471	9.87324	9.86777	9.87798	
$\eta_b(2S)^*$	$2\,^1S_0$	0^{-+}	9.999	10.03214	10.03214	10.03214	10.03214	0.46047
$\Upsilon(2S)^*$	$2\,^3S_1$	1^{--}	10.02326	10.04925	10.03120	10.02216	10.04925	0.45700
	$1\,^3D_1$	1^{--}		10.11883	10.11464	10.11254	10.11883	0.01827
$\Upsilon(1D)^*$	$1\,^3D_2$	2^{--}	10.1637	10.12300	10.12834	10.12300	10.12990	
	$1\,^1D_2$	2^{-+}		10.14099	10.13816	10.13710	10.14099	
	$1\,^3D_3$	3^{--}		10.14346	10.13838	10.13081	10.14346	
$\chi_{b0}(2P)^*$	$2\,^3P_0$	0^{++}	10.2325	10.27462	10.27462	10.27462	10.27462	0.
$h_b(2P)^*$	$2\,^1P_1$	1^{+-}	10.2598	10.33064	10.32905	10.32825	10.33064	0.
$\chi_{b1}(2P)^*$	$2\,^3P_1$	1^{++}	10.25546	10.28884	10.30469	10.28884	10.31260	0.03509
$\chi_{b2}(2P)^*$	$2\,^3P_2$	2^{++}	10.26865	10.33363	10.32740	10.31715	10.33452	
	$1\,^3F_2$	2^{++}		10.36803	10.35942	10.35435	10.36803	
	$1\,^3F_3$	3^{++}		10.37062	10.37225	10.36921	10.37571	
	$1\,^1F_3$	3^{+-}		10.38509	10.37936	10.37683	10.38509	
	$1\,^3F_4$	4^{++}		10.38710	10.37873	10.36791	10.38710	
	$3\,^1S_0$	0^{-+}		10.49843	10.49843	10.49843	10.49843	0.43906
$\Upsilon(3S)^*$	$3\,^3S_1$	1^{--}	10.3552	10.51176	10.49099	10.48059	10.51176	0.44228
	$2\,^3D_1$	1^{--}		10.55174	10.54460	10.54102	10.55174	0.02241
	$2\,^3D_2$	2^{--}		10.55509	10.56334	10.55509	10.56747	
	$2\,^1D_2$	2^{-+}		10.58458	10.57689	10.57415	10.58458	
	$2\,^3D_3$	3^{--}		10.58627	10.57435	10.56074	10.58627	

	$1\,^3G_3$	3^{--}		10.60407	10.58968	10.58107	10.60407	
	$1\,^3G_4$	4^{--}		10.60613	10.58410	10.54711	10.61116	
	$1\,^1G_4$	4^{-+}		10.61971	10.60863	10.60269	10.61971	
	$1\,^3G_5$	5^{--}		10.62171	10.60776	10.59234	10.62171	
$\chi_{b?}(3P)$	$3\,^3P_0$	0^{++}	10.5794	10.70393	10.70393	10.70393	10.70393	0.
	$3\,^3P_1$	1^{++}		10.71532	10.73571	10.71532	10.74589	0.04951
	$3\,^1P_1$	1^{+-}		10.76921	10.76330	10.76034	10.76921	0.
	$3\,^3P_2$	2^{++}		10.77023	10.75765	10.74316	10.77023	
	$4\,^1S_0$	0^{-+}		10.93561	10.93561	10.93561	10.93561	0.41974
$\Upsilon(4S)$	$4\,^3S_1$	1^{--}	10.5794	10.94581	10.92267	10.91109	10.94581	0.42446

* States whose masses are used to fit the parameters κ and m_b in this work.

[1] K.A. Olive et al. (Particle Data Group), Chin. Phys. C **38**, 090001 (2014); [http://pdg.lbl.gov].

Table 7: The bottomonium spectrum and decay constants ($N_{\max} = L_{\max} = 24, \kappa = 1.490\,\mathrm{GeV}, m_b = 4.763\,\mathrm{GeV}$). $M_{\rm pdg}$ quotes bottomonium masses from Particle Data Group[1] (PDG 2014). $M_{m_J=0}$ collects the masses from the $m_J = 0$ sector. The r.m.s. average-m_J mass $\overline{M} = \left[(M_{-J}^2 + M_{1-J}^2 + \cdots + M_{+J}^2)/(2J+1)\right]^{\frac{1}{2}}$. $M_{\min} = \min\{M_{m_J}\}$, $M_{\max} = \max\{M_{m_J}\}$.

	$n\,^{2S+1}L_J$	J^{PC}	$M_{\rm pdg}$(GeV)	$M_{m_J=0}$(GeV)	$\overline{M}$(GeV)	$M_{\min}$(GeV)	$M_{\max}$(GeV)	f(GeV)
$\eta_b(1S)^*$	$1\,^1S_0$	0^{-+}	9.398	9.49182	9.49182	9.49182	9.49182	0.57499
$\Upsilon(1S)^*$	$1\,^3S_1$	1^{--}	9.4603	9.52401	9.50588	9.49680	9.52401	0.53223
$\chi_{b0}(1P)^*$	$1\,^3P_0$	0^{++}	9.85944	9.82570	9.82570	9.82570	9.82570	0.
$\chi_{b1}(1P)^*$	$1\,^3P_1$	1^{++}	9.89278	9.84297	9.85371	9.84297	9.85907	0.00766
$h_b(1P)^*$	$1\,^1P_1$	1^{+-}	9.8993	9.87168	9.87301	9.87168	9.87367	0.
$\chi_{b2}(1P)^*$	$1\,^3P_2$	2^{++}	9.91221	9.87680	9.87533	9.86982	9.88009	
$\eta_b(2S)^*$	$2\,^1S_0$	0^{-+}	9.999	10.02867	10.02867	10.02867	10.02867	0.49181
$\Upsilon(2S)^*$	$2\,^3S_1$	1^{--}	10.02326	10.04909	10.02950	10.01969	10.04909	0.48152
	$1\,^3D_1$	1^{--}		10.12060	10.11636	10.11424	10.12060	0.01891
$\Upsilon(1D)^*$	$1\,^3D_2$	2^{--}	10.1637	10.12479	10.13013	10.12479	10.13172	
	$1\,^1D_2$	2^{-+}		10.14277	10.13996	10.13891	10.14277	
	$1\,^3D_3$	3^{--}		10.14525	10.14019	10.13264	10.14525	
$\chi_{b0}(2P)^*$	$2\,^3P_0$	0^{++}	10.2325	10.27171	10.27171	10.27171	10.27171	0.
$\chi_{b1}(2P)^*$	$2\,^3P_1$	1^{++}	10.25546	10.28761	10.30453	10.28761	10.31298	0.02967
$h_b(2P)$	$2\,^1P_1$	1^{+-}	10.2598	10.33154	10.32993	10.32912	10.33154	0.
$\chi_{b2}(2P)^*$	$2\,^3P_2$	2^{++}	10.26865	10.33473	10.32853	10.31821	10.33575	
	$1\,^3F_2$	2^{++}		10.36949	10.36092	10.35586	10.36949	
	$1\,^3F_3$	3^{++}		10.37208	10.37371	10.37070	10.37714	
	$1\,^1F_3$	3^{+-}		10.38651	10.38082	10.37831	10.38651	
	$1\,^3F_4$	4^{++}		10.38852	10.38020	10.36941	10.38852	
	$3\,^1S_0$	0^{-+}		10.49364	10.49364	10.49364	10.49364	0.47294
$\Upsilon(3S)^*$	$3\,^3S_1$	1^{--}	10.3552	10.51028	10.48765	10.47632	10.51028	0.47155
	$2\,^3D_1$	1^{--}		10.55258	10.54524	10.54157	10.55258	0.02352
	$2\,^3D_2$	2^{--}		10.55602	10.56429	10.55602	10.56834	
	$2\,^1D_2$	2^{-+}		10.58552	10.57790	10.57517	10.58552	
	$2\,^3D_3$	3^{--}		10.58730	10.57542	10.56180	10.58730	
	$1\,^3G_3$	3^{--}		10.60517	10.59085	10.58226	10.60517	
	$1\,^3G_4$	4^{--}		10.60722	10.60423	10.59558	10.61220	
	$1\,^1G_4$	4^{-+}		10.62070	10.60975	10.60385	10.62070	
	$1\,^3G_5$	5^{--}		10.63009	10.60955	10.59352	10.63009	
$\chi_{b?}(3P)$	$3\,^3P_0$	0^{++}	10.5794	10.69830	10.69830	10.69830	10.69830	0.
	$3\,^3P_1$	1^{++}		10.71193	10.73392	10.71193	10.74490	0.04780
	$3\,^1P_1$	1^{+-}		10.76906	10.76307	10.76007	10.76906	0.
	$3\,^3P_2$	2^{++}		10.77028	10.75775	10.74307	10.77028	
	$4\,^1S_0$	0^{-+}		10.92944	10.92944	10.92944	10.92944	0.45811
$\Upsilon(4S)$	$4\,^3S_1$	1^{--}	10.5794	10.94290	10.91748	10.90475	10.94290	0.45977

* States whose masses are used to fit the parameters κ and m_b in this work.

[1] K.A. Olive et al. (Particle Data Group), Chin. Phys. C **38**, 090001 (2014); [http://pdg.lbl.gov].

Table 8: The masses, decay constants for pseudo-scalar and (axial-)vector quarkonia[1]. See Table 1 for model parameters. The masses are taken from the r.m.s. average-m_J values $\overline{M}$. The decay constants are computed using the light-front wavefunction of the $m_J = 0$ sector. The decay constants are also extrapolated (extr.) using simple polynomials in $N_{\max}^{-1}$.

		mass $\overline{M}$ (MeV), $N_{\max} = 8, 16, 24$				decay constant (MeV), $N_{\max} = 8, 16, 24$				
		PDG[2]	**I** (8)	**II** (16)	**III** (24)	PDG[2ab]	**I** (8)	**II** (16)	**III** (24)	extr.
0^{-+}	$\eta_c(1S)$	2983.6	3080	3073	3069	330±13	361	401	423	482
	$\eta_c(2S)$	3639.4	3697	3680	3668	238^{+72}_{-104}	295	322	330	345
	$\eta_b(1S)$	9398.0	9502	9495	9492		470	539	575	665
	$\eta_b(2S)$	9999.0	10040	10032	10029		393	460	492	568
	$\eta_b(3S)$		10512	10498	10494		358	439	473	551
1^{--}	J/ψ	3096.916	3110	3123	3134	407±5	351	372	380	394
	$\psi(2S)$	3686.109	3687	3679	3676	290±2	301	333	344	366
	$\psi(3770)$	3773.155	3728	3733	3735	97.7±3	78	87	89	94
	$\Upsilon(1S)$	9460.3	9510	9507	9506	689±5	457	510	532	585
	$\Upsilon(2S)$	10023.3	10037	10031	10030	479±4	397	457	482	537
	$\Upsilon(3S)$	10355.2	10504	10491	10488	414±4	364	442	472	535
	$\Upsilon(1^3D_1)$		10110	10115	10116		17	18	19	21
	$\Upsilon(2^3D_1)$		10544	10545	10545		24	22	24	28
1^{++}	$\chi_{c1}(1P)$	3510.66	3443	3450	3455		62	59	54	38
	$\chi_{b1}(1P)$	9892.78	9849	9852	9854		26	15	8	0*
	$\chi_{b1}(2P)$	10255.46	10306	10305	10305		39	35	30	13
	$\chi_{b1}(3P)$		10743	10736	10734		44	50	48	39

* The naïve extrapolation yields a negative value ($-14\,\mathrm{MeV}$), which is corrected to 0, as the quantity should be positive.

[1] The decay constants of 0^{++} (scalar meson) and 1^{+-} (h axial vector meson) are exactly zero due to charge conjugation symmetry.

[2] K.A. Olive et al. (Particle Data Group), Chin. Phys. C **38**, 090001 (2014); [`http://pdg.lbl.gov`].

[a] For pseudo scalars (0^{-+}), the decay constants are extracted from the diphoton decay width according to[3–4],

$$\Gamma_{P\to\gamma\gamma} = \frac{\pi}{4}\alpha_{\rm em}^2 e_Q^4 m_P^3 \left|F_{P\gamma}(0)\right|^2 = 4\pi e_Q^4 \alpha_{\rm em}^2 \frac{f_P^2}{m_P},$$

where e_Q is the charge number of the constituent quark ($e_Q = 2/3$ for charm quark and $e_Q = -1/3$ for bottom quark), m_P is the mass of the pseudo scalar, $\alpha_{\rm em} = \alpha_{\rm em}(Q)$ is the QED running coupling. For charmonium, we take $\alpha_{\rm em}(3.5\,\mathrm{GeV}) \simeq 1/134$; for bottomonium, we take $\alpha_{\rm em}(9.5\,\mathrm{GeV}) \simeq 1/132$. The higher order pQCD correction is assumed to be included in the non-perturbative dynamics of the bound states.

[b] For vector mesons (1^{--}), the decay constants are extracted from the dilepton decay width according to[3–4],

$$\Gamma_{V\to e^+e^-} = \frac{4\pi}{3} e_Q^2 \alpha_{\rm em}^2 \frac{f_V^2}{m_V}.$$

where m_V is the mass of the vector meson.

[3] S. Godfrey and N. Isgur, Phys. Rev. D **32**, 189 (1985).

[4] C.T.H. Davies, C. McNeile,E. Follana, G.P. Lepage, H. Na, and J. Shigemitsu (HPQCD collaboration), Phys. Rev. D **82**, 114504 (2010).